Pergamon

Geochimica et Cosmochimica Acta, Vol. 66, No. 4, pp. 635–646, 2002

0016-7037/−1898 $22.00 + .00

PII S0016-7037(01)00793-1

Energetics of multicomponent diffusion in molten CaO-Al_2O_3-SiO_2

YAN LIANG[1,*] and ANDREW M. DAVIS[2]

[1]Department of the Geological Sciences, Brown University, Providence, RI 02912, USA [2]Department of the Geophysical Sciences and Enrico Fermi Institute, The University of Chicago, Chicago, IL 60637, USA

(*Received January* 5, 2001; *accepted in revised form August* 13, 2001)

Abstract—The energetics of multicomponent diffusion in molten CaO-Al_2O_3-SiO_2 (CAS) were examined experimentally at 1440 to 1650°C and 0.5 to 2 GPa. Two melt compositions were investigated: a haplodacitic melt (25 wt.% CaO, 15% Al_2O_3, and 60% SiO_2) and a haplobasaltic melt (35% CaO, 20% Al_2O_3, and 45% SiO_2). Diffusion matrices were measured in a mass-fixed frame of reference with simple oxides as end-member components and Al_2O_3 as a dependent variable. Chemical diffusion in molten CAS shows clear evidence of diffusive coupling among the components. The diffusive flux of SiO_2 is significantly enhanced whenever there is a large CaO gradient that is oriented in a direction opposite to the SiO_2 gradient. This coupling effect is more pronounced in the haplodacitic melt and is likely to be significant in natural magmas of rhyolitic to andesitic compositions. The relative magnitude of coupled chemical diffusion is not very sensitive to changes in temperature and pressure.

To a good approximation, the measured diffusion matrices follow well-defined Arrhenius relationships with pressure and reciprocal temperature. Typically, a change in temperature of 100°C results in a relative change in the elements of diffusion matrix of 50 to 100%, whereas a change in pressure of 1 GPa introduces a relative change in elements of diffusion matrix of 4 to 6% for the haplobasalt, and less than 5% for the haplodacite. At a pressure of 1 GPa, the ratios between the major and minor eigenvalues of the diffusion matrix λ_1/λ_2 are not very sensitive to temperature variations, with an average of 5.5 ± 0.2 for the haplobasalt and 3.7 ± 0.6 for the haplodacite. The activation energies for the major and minor eigenvalues of the diffusion matrix are 215 ± 12 and 240 ± 21 kJ mol^{-1}, respectively, for the haplodacite and 192 ± 8 and 217 ± 14 kJ mol^{-1} for the haplobasalt. These values are comparable to the activation energies for self-diffusion of calcium and silicon at the same melt compositions and pressure. At a fixed temperature of 1500°C, the ratios λ_1/λ_2 increase with the increase of pressure, with λ_1/λ_2 varying from 2.5 to 4.1 (0.5 to 1.3 GPa) for the haplodacite and 4 to 6.5 (0.5 to 2.0 GPa) for the haplobasalt. The activation volumes for the major and minor eigenvalues of the diffusion matrix are 0.31 ± 0.44 and 2.3 ± 0.8 cm^3 mol^{-1}, respectively, for the haplodacite and –1.48 ± 0.18 and –0.42 ± 0.24 cm^3 mol^{-1} for the haplobasalt. These values are quite different from the activation volumes for self-diffusion of calcium and silicon at the same melt compositions and temperature. These differences in activation volumes between the two melts likely result from a difference in the structure and thermodynamic properties of the melt between the two compositions (e.g., partial molar volume).

Applications of the measured diffusion matrices to quartz crystal dissolution in molten CAS reveal that the activation energy and activation volume for quartz dissolution are almost identical to the activation energy and activation volume for diffusion of the minor or slower eigencomponent of the diffusion matrix. This suggests that the diffusion rate of slow eigencomponent is the rate-limiting factor in isothermal crystal dissolution, a conclusion that is likely to be valid for crystal growth and dissolution in natural magmas when diffusion in liquid is the rate-limiting factor.

1. INTRODUCTION

Chemical diffusion in molten silicate has played a key role in many petrological and geochemical mass transfer processes involving crystal-melt and melt-melt interactions. The rate of crystal dissolution in a melt, for example, is determined by the rate of diffusion in the liquid, the thickness of concentration boundary, and the extent of undersaturation of the melt (e.g., Cooper and Kingery, 1964; Watson, 1982; Zhang et al., 1989; Watson and Baker, 1991; Kerr, 1995; Liang, 2000). Chemical diffusion in natural magmas is multicomponent in that the flux of a given component, say SiO_2, is a linear combination of the concentration gradients of the independent components in the system. This is Onsager's extension of Fick's first law of diffusion. In a mass-fixed (barycentric) frame of reference the diffusive flux of component i in an n-component liquid, J_i, is given by (e.g., Onsager, 1945, de Groot and Mazur, 1962; Haase, 1969)

$$J_i = -\rho\sum_{j=1}^{n-1} D_{ij}\nabla C_j, \tag{1}$$

where ρ is melt density; D_{ij} are elements of an $(n-1)\times(n-1)$ diffusion matrix, [**D**], with component n taken as the dependent variable; and C_j is mass fraction of component j. In the absence of a sink or source and bulk flow, mass conservation in a fluid volume element leads to the multicomponent diffusion equation

$$\rho\frac{\partial C_i}{\partial t} = \sum_{j=1}^{n-1}\nabla\cdot(\rho D_{ij}\nabla C_j). \tag{2}$$

*Author to whom correspondence should be addressed (yan_liang@brown.edu).

When the density and composition variations in a melt of interest are small, Eqn. 2 can be simplified by neglecting the nonlinear terms $\nabla(\rho D_{ij}) \cdot \nabla C_j$, namely,

$$\frac{\partial C_i}{\partial t} = \sum_{j=1}^{n-1} D_{ij} \nabla^2 C_j . \quad (3)$$

The neglected terms are of order $\Delta D_{ij}/D$ and $\Delta\rho/\rho_0$when compared with the order-one term on the left-hand side of Eqn. 3 and are small in many practical applications, where ΔD_{ij} and $\Delta\rho$ are magnitudes of diffusivity and density variations in the melt, respectively; D is a characteristic diffusivity; and ρ_0 is the average melt density (e.g., Richter et al., 1998). In a ternary system, the full expressions of Eqn. 3 are

$$\frac{\partial C_1}{\partial t} = D_{11} \nabla^2 C_1 + D_{12} \nabla^2 C_2, \quad (4a)$$

$$\frac{\partial C_2}{\partial t} = D_{21} \nabla^2 C_1 + D_{22} \nabla^2 C_2, \quad (4b)$$

where component 3 is taken as the dependent variable. Diffusion matrices at selected compositions for a number of simple molten silicate systems of petrologic interest have been reported: CaO-Al_2O_3-SiO_2 (CAS) (Sugawara et al., 1977; Oishi et al., 1982; Liang et al., 1996b), MgO-Al_2O_3-SiO_2 and CaO-MgO-Al_2O_3-SiO_2 (CMAS) (Kress and Ghiorso, 1993; Richter et al., 1998), K_2O-Al_2O_3-SiO_2 (Chakraborty et al., 1995), K_2O-SrO-SiO_2 (Varshneya and Cooper, 1972), Na_2O-CaO-SiO_2 (Wakabayashi and Oishi, 1978, with diffusion matrix given by Trial and Spera, 1994), and K_2O-NaO-Al_2O_3-SiO_2-H_2O (Mungall et al., 1998). In two recent studies (Liang et al., 1996a, 1996b), we measured the composition dependence of self-diffusion coefficients and multicomponent diffusion coefficients in molten CAS at 1500°C and 1 GPa. The primary purpose of these two studies was to obtain a complete data set of diffusion parameters that would allow us to test and validate empirical multicomponent diffusion models (Liang et al., 1997). In a more recent study, we showed that the measured multicomponent diffusion coefficients can be used to predict quartz diffusive dissolution rate and interface melt composition in molten CAS once the quartz liquidus is known (Liang, 1999). In this paper, we report the temperature and pressure dependence of multicomponent diffusion coefficients in molten CAS at two melt compositions: a haplodacite (25 wt.% CaO, 15% Al_2O_3, and 60% SiO_2; composition 7 in Fig. 1) and a haplobasalt (35% CaO, 20% Al_2O_3, and 45% SiO_2; composition 12 in Fig. 1). By knowing the temperature, pressure, and composition dependence of chemical diffusion coefficients, we will have a complete set of diffusion parameters for modeling any diffusion-related mass transport problems in molten CAS, which is one of the simplest multicomponent systems that bears key components of natural magmas.

A brief description of materials and methods is given in the next section. Experimentally measured multicomponent diffusion coefficients at the two melt compositions in the ternary system CAS at temperatures of 1440 to 1650°C and pressures of 0.5 to 2 GPa are presented under "Results." Energetics of chemical diffusion are discussed under "Discussion," where activation energies and activation volumes are evaluated for melts of different compositions and compared with values reported for other simple systems. And finally, an example of how the measured chemical diffusion coefficients can be used to evaluate the energetics of crystal dissolution is given under "Geological Applications."

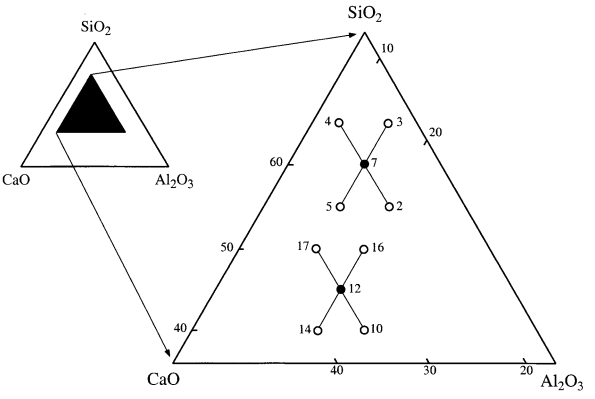

Fig. 1. Composition space relevant to the chemical diffusion studies in molten CaO-Al_2O_3-SiO_2. Diffusion matrices were measured at composition 7 (25 wt.% CaO, 15% Al_2O_3, and 60% SiO_2) and composition 12 (35% CaO, 20% Al_2O_3, and 45% SiO_2, filled circles). Open circles mark the starting compositions used to form diffusion couples. For example, compositions 4 and 2 and compositions 3 and 5 (joined by tie lines) form two diffusion couples around composition 7.

2. EXPERIMENTAL METHODS

Starting compositions for the chemical diffusion experiments in the ternary system CAS reported below were from our earlier diffusion studies (Liang et al., 1996a; 1996b). Figure 1 shows the compositions (wt.%) that were used to form the chemical diffusion couples (open and filled circles around compositions 7 and 12). Nominal compositions were given in Liang et al. (1996a; 1996b).

Chemical diffusion experiments were carried out in a 3/4-inch piston cylinder apparatus in much the same way as the diffusion experiments described in Liang et al. (1996a; 1996b). Diffusion couples were formed by firmly packing glass powders of one starting composition against another in one of the two predrilled holes (1.4 to 2 mm inside diameter, 7.5 to 9.0 mm long) in a molybdenum capsule. No platinum liner was used in these setups because the exchange between the molybdenum sidewall and the melts used in this study is negligibly small ($<$50 ppm) for the run duration used in this study ($\leq$2.5 h). To avoid convection, less dense starting compositions were placed on top of the denser ones. To start a diffusion experiment, a diffusion capsule was first pressurized cold to a pressure 10 to 20% higher than the desired pressure in the piston cylinder apparatus. The temperature was then raised at a rate of 75°C min^{-1} up to 1000°C and 100 to 300°C min^{-1} to the run temperature (1440 to 1650°C). At the end of the run, the temperature was first dropped to 600°C by a step change in temperature (which takes $\sim$10 s) while maintaining the pressure at approximately the experimental run pressure. The charge was then held at 600°C for $\sim$2 min before a final quench to room temperature. The purpose of this two-step quench is to minimize dilation cracks. The quenched capsules were then sectioned longitudinally, polished, and mounted for electron microprobe analysis.

The temperature was measured with a $W_{97}Re_3$-$W_{75}Re_{25}$ thermocouple and a Eurotherm 818 controller. This system maintains temperature to within 3°C of a desired run temperature. No pressure correction was applied to the measured e.m.f. Uncertainties in temperature measurements were $\sim$10°C. This is due mainly to the presence of a temperature gradient in the furnace (e.g., Ayers et al., 1992). The nominal pressure was not corrected for friction because pressure fluctuations during a typical run were comparable to the friction correction measured by

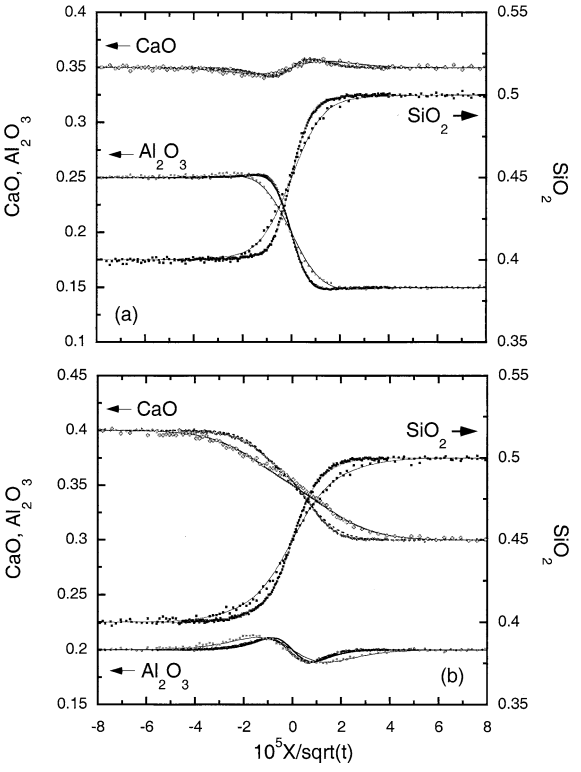

Fig. 2. Plots of measured concentration profiles as a function of $10^5 X/\sqrt{t}$ (in m $s^{-1/2}$) for two representative runs, CDT-12-2 (1570°C, 1 GPa, and 0.2 h) and CDT-12-4 (1440°C, 1 GPa, and 0.6 h). Solid lines are calculated diffusion profiles using the exact solutions of Fujita and Gosting (1956) and Kirkaldy (1958) and measured diffusion matrices at the two temperatures (Table 1).

Ayers et al. (1992) for a similar furnace assemblage (~25 MPa). Pressure correction at 0.5 GPa is somewhat larger (20 to 30%, based on our preliminary NaCl melting experiments).

Most of the chemical diffusion profiles were collected using either a Cameca SX-50 electron microprobe at the University of Chicago or a JEOL 730 electron microprobe at Rensselaer Polytechnic Institute. Several chemical diffusion profiles were measured at the University of Chicago using a JEOL-5800LV scanning electron microscope equipped with an Oxford Link ISIS-300 X-ray microanalysis system. Operating conditions for electron microprobe were an accelerating voltage of 15 kV, a beam current of 25 nA, a beam spot of 5 μm, and a counting time of 30 s. Operating conditions for scanning electron microscopy were an accelerating voltage of 15 kV and a beam current of 15 nA. Under these conditions, precisions of ~0.3% relative for major elements can be demonstrated on the flat portions of diffusion profiles. Representative chemical diffusion profiles are shown in Figures 2a and 2b.

3. RESULTS

The temperature and pressure dependence of chemical diffusion matrices in molten CAS were investigated for two melts: composition 7 (25 wt.% CaO, 15% Al_2O_3, and 60% SiO_2) and composition 12 (35% CaO, 20% Al_2O_3, and 45% SiO_2). Two diffusion couples were used at each melt composition: diffusion couples 4/2 and 3/5 (top/bottom) for composition 7 and diffusion couples 16/14 and 17/10 for composition 12 (Fig. 1). Use of two diffusion couples around each melt composition allows us to better constrain the diffusion matrices in the ternary system (e.g., Varshneya and Cooper, 1972; Liang, 1994; Trial and Spera, 1994). Figures 2a and 2b present the measured concentration profiles as a function of distance normalized by the square root of time (10^5 $X/\sqrt{t}$ for two runs around composition 12 (CDT-12-2, 1570°C and 1 GPa, and CDT-12-4, 1440°C and 1 GPa). (An example of measured concentration profiles in diffusion couples 4/2 and 3/5 can be found in Figs. 3a and 3b of Liang et al., 1996b.) In diffusion couple 17/10 (Figs. 1 and 2a), the concentration of CaO was initially uniform across the interface. Diffusive exchange between compositions 17 and 10 was dominated by concentration gradients of SiO_2 and Al_2O_3. In diffusion couple 16/14 (Figs. 1 and 2b), the concentration of Al_2O_3 was initially uniform. Diffusive exchange between compositions 16 and 14 was dominated by the concentration gradient of CaO, and to a lesser extent the concentration gradient SiO_2, as will be shown below. These diffusive exchanges are strongly coupled in that concentration gradients of CaO in Figure 2a, for example, are affected by concentration gradients of SiO_2 (if Al_2O_3 is taken as the dependent variable). The apparent diffusion rate of SiO_2 is enhanced by the presence of a CaO concentration gradient (cf. Figs. 2a and 2b). These, as well as the uphill diffusion profiles of CaO in Figure 2a and Al_2O_3 in Figure 2b, are results of coupled chemical diffusion, and can be fully accounted for by a diffusion matrix defined in Eqn. 4.

Table 1 and Figures 3 and 4 summarize the measured diffusion matrices as a function of temperature and run pressure for the two melt compositions when Al_2O_3 (designated as component 3) is taken as the dependent variable. (CaO is taken as component 1 and SiO_2 as component 2.) These diffusion matrices were obtained from a simultaneous inversion of concentration profiles along two directions in the composition space following the same procedure as in Liang (1994) and Liang et al. (1996b). The sources of error for the chemical diffusion coefficients given in Table 1 are due mainly to uncertainties in temperature measurements and capsule deformation during the run (e.g., Liang et al., 1996a; 1996b; also see below). The relative 1σ errors for the elements of the diffusion matrix around compositions 7 and 12 are approximately 10 to 15% for D_{11} and D_{22} and 20 to 25% for D_{12} and D_{21}. Figures 2a and 2b show good agreement between the calculated concentration profiles (solid lines) using appropriate diffusion matrices listed in Table 1 and the measured concentration profiles in the two runs (circles and squares). Figures 3 and 4 show that to a good approximation, temperature and pressure dependence of the measured diffusion matrices can be parameterized using the exponential relationships

$$D_{ij} = A_1 \exp\left(-\frac{10000A_2}{T}\right), \tag{5a}$$

$$D_{ij} = B_1 \exp(B_2 P), \tag{5b}$$

where T is the absolute temperature, P is in GPa, and D_{ij} is in m^2 s^{-1}. Coefficients A_1, A_2, B_1, and B_2 are listed in Table 2. Overall, a change in temperature of 10°C gives rise to a relative change in elements of diffusion matrix of 5 to 10% over the temperature range of 1440 to 1650°C. A change in pressure of

Table 1. List of chemical diffusion coefficients taking Al_2O_3 as the dependent variable.

Composition	T (°C)	P (GPa)	Time (h)	D_{11}	D_{12}	D_{21}	D_{22}	Run number
7	1450	1.0	2.5	2.51	0.22	–1.18	0.45	CDT-7-1
	1500	1.0		4.66	0.44	–2.68	1.00	[1][a]
	1570	1.0	0.5	8.16	0.93	–3.52	1.59	CDT-7-4
	1650	1.0	0.2	13.40	1.90	–6.29	2.28	CDT-7-3
	1500	0.5	1.5	4.16	0.50	–1.92	0.93	CDP-7-2
	1500	1.3	1.0	3.91	0.47	–1.77	0.67	CDT-7-3
	1500	1.3	1.0	4.50	0.61	–2.11	0.64	CDP-7-4
12	1440	1.0	0.6	7.40	–2.55	–2.98	2.97	CDT-12-4
	1450	1.0	0.6	9.29	–3.39	–3.69	3.62	CDT-12-1
	1500	1.0	0.5	12.34	–2.26	–2.97	4.28	CD-10[b]
	1500	1.0	0.3	11.85	–3.45	–4.44	4.90	CD-15
	1570	1.0	0.2	21.37	–6.11	–8.06	7.67	CDT-12-2
	1650	1.0	0.1	34.52	–11.08	–12.02	14.86	CDT-12-3
	1500	0.5	0.3	10.51	–2.89	–3.54	4.27	CDP-12-5
	1500	1.5	0.3	13.13	–4.77	–6.22	6.54	CDP-12-15
	1500	2.0	0.3	17.73	–5.97	–11.52	8.27	CDP-12-20

Diffusion coefficients in 10^{-11} m^2s^{-1}, component 1 = CaO, component 2 = SiO_2.
[a] Average of two runs from Liang et al. (1996b).
[b] From Liang et al. (1996b).

100 MPa, on the other hand, results in a relative change in elements of diffusion matrix of 4 to 8% for composition 12, and less than 5% for composition 7. Hence, errors in pressure calibration will not significantly affect the measured [**D**] for the two melt compositions examined in this study.

4. DISCUSSION

4.1. Diffusive Coupling

One of the key features of chemical diffusion in a multicomponent system is coupled diffusion. The nature and extent of

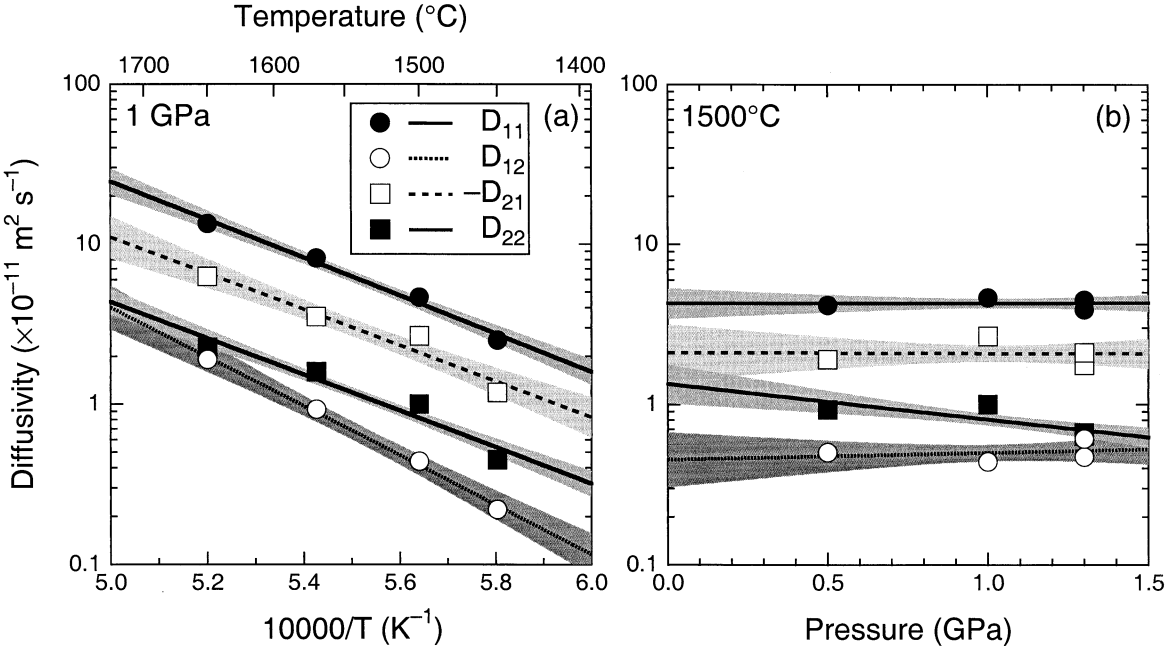

Fig. 3. Plots of measured elements of diffusion matrices at composition 7 as a function of temperature (1 GPa, panel [a]) and pressure (1500°C, panel [b]). The diffusion matrices were calculated with Al_2O_3 as the dependent variable (component 3), CaO as component 1, and SiO_2 as component 2. Elements of diffusion matrices are shown as filled circles (D_{11}), open circles (D_{12}), open squares ($-D_{21}$), and filled squares (D_{22}). Use of $-D_{21}$ in the semilog plot is because measured $D_{21} < 0$. Solid or dashed lines represent the exponential fits to the measured data (regression coefficients are listed in Table 2). One-σ error hyperbolas are also shown for each regression line. The error hyperbolas were calculated using an uncertainty of 12.5% relative for D_{11} and D_{22}, 22.5% relative for D_{12} and D_{21}, 10°C for temperature, 0.125 GPa for runs at 0.5 GPa, and 0.1 GPa for all other runs.

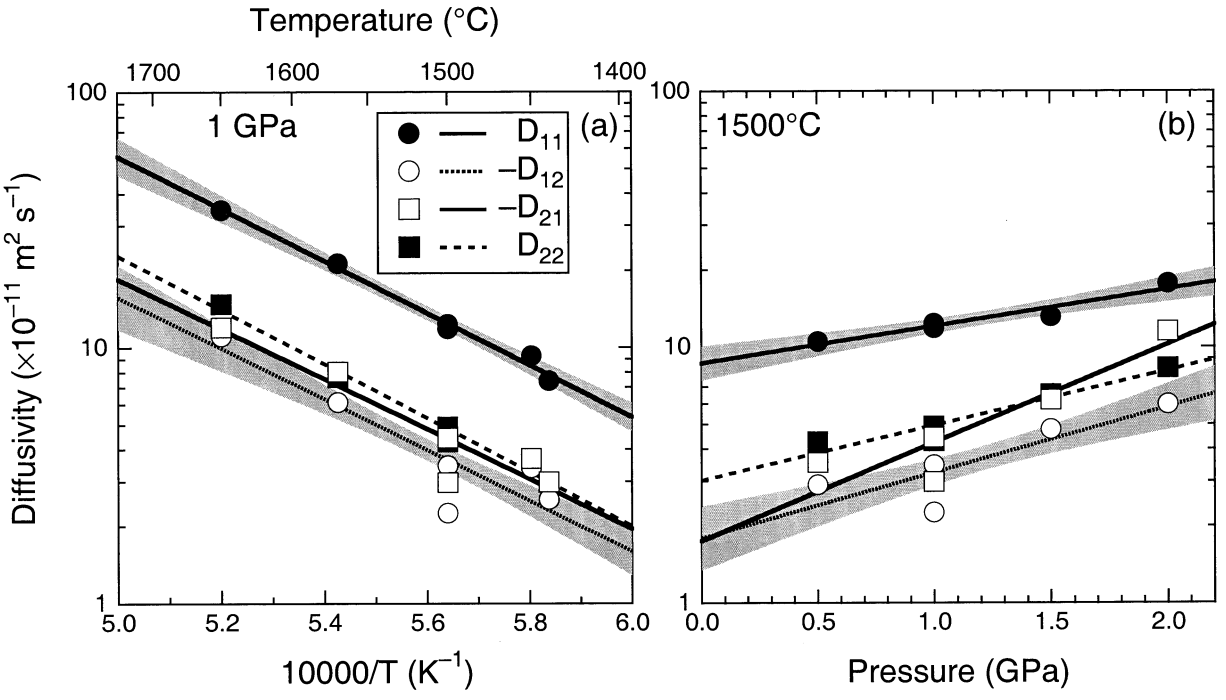

Fig. 4. Plots of measured elements of diffusion matrices at composition 12 as a function of temperature (1 GPa, panel [a]) and pressure (1500°C, panel [b]). CaO and SiO_2 are designated as components 1 and 2, respectively. Al_2O_3 is taken as the dependent variable (component 3). Filled circles represent measured D_{11}, open circles are $-D_{12}$, open squares are $-D_{21}$, and filled squares are D_{22}. Measured D_{12} and D_{21} are less than zero. Solid or dashed lines represent the exponential fits to the measured data (regression coefficients are listed in Table 2). For clarity, 1σ error hyperbolas for D_{12} and D_{21} are not shown (see caption of Fig. 3 for details).

coupled chemical diffusion can be easily understood if we compare the relative magnitudes of the two terms on the right-hand side of Eqn. 4a or 4b. The flux of component 2 (SiO_2) is strongly coupled to the concentration gradients of component 1 (CaO) if $|D_{21}\Delta C_1|<|D_{22}\Delta C_2|$, where ΔC_1 and ΔC_2 are magnitudes of concentration variations across a diffusion couple for component 1 and component 2, respectively. Similarly, the flux of component 1 is strongly coupled to the concentration gradient of component 2 if $|D_{11}\Delta C_1|<|D_{12}\Delta C_2|$. For the temperature and pressure ranges examined in this study, the ratio $|D_{21}/D_{22}|$ varies between 2 and 6 for composition 7, and between 0.7 and 1 for composition 12. Hence, the flux of SiO_2 is strongly coupled to the concentration gradients of CaO except when the concentration gradients of CaO are very small compared to the concentration gradients of SiO_2 (cf. Figs. 2a and 2b). This coupling effect is more pronounced for melts of more siliceous compositions, which is consistent with our earlier observations of the compositional dependence of multicomponent diffusion in CAS at 1500°C and 1 GPa (Liang et al., 1996b). Given the very small ratios of D_{12}/D_{11} for composition 12 (~ -0.3) and composition 7 (~ 0.2), the flux of CaO is strongly affected by the concentration gradients of SiO_2 when concentration variation in SiO_2 is much larger than that in CaO. This is the case for diffusion couples 17/10 (Fig. 2a) and 4/2.

Table 2. List of coefficients for Eqn. 5a and 5b.

Composition	[D]	A_1[a]	A_2	B_1	B_2
7	D_{11}	2.1	2.74 ± 0.33	4.28	0.00 ± 0.20
	D_{12}	20.1	3.55 ± 0.56	0.45	0.10 ± 0.36
	$-D_{21}$	4.6	2.59 ± 0.54	2.12	0.01 ± 0.38
	D_{22}	2.1	2.61 ± 0.33	1.35	0.51 ± 0.26
12	D_{11}	7.0	2.35 ± 0.27	8.66	–0.33 ± 0.12
	$-D_{12}$	1.5	2.29 ± 0.46	1.79	–0.59 ± 0.22
	$-D_{21}$	1.4	2.25 ± 0.45	1.75	–0.89 ± 0.23
	D_{22}	4.4	2.43 ± 0.27	3.01	–0.50 ± 0.13

Component 1 = CaO, component 2 = SiO_2.
[a] A_1 in 10^{-5} m^{2}s^{-1}.

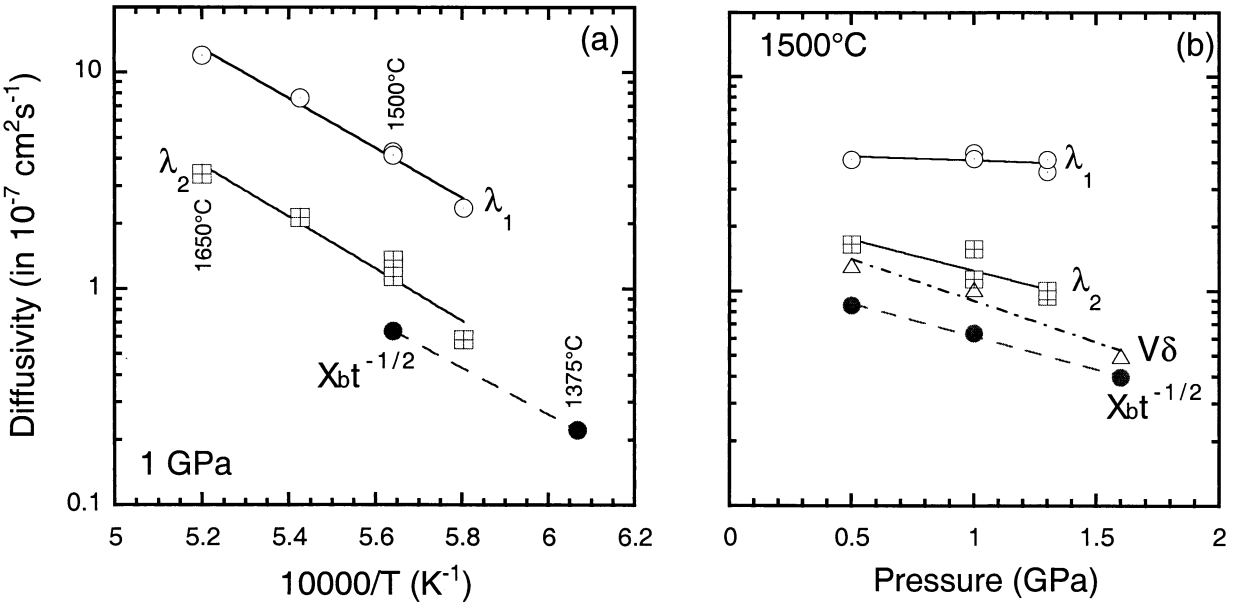

Fig. 5. Plots of major (λ_1, open circles) and minor (λ_2, squares) eigenvalues of diffusion matrices at composition 7 as a function of temperature (1 GPa, panel [a]) and pressure (1500°C, panel [b]). Exponential fits to the measured data are shown as solid lines. For comparison, calculated quartz diffusive dissolution distances (normalized by square root of time) are also shown (filled circles). The normalized dissolution distances were calculated using independently measured quartz liquidus (Table 4) and diffusion matrices at composition 7. Composition of the dissolving melt is 30% CaO, 20% Al_2O_3, and 50% SiO_2 (composition 16 in Fig. 1). Also shown in panel (b) are calculated products of quartz convective dissolution rate (V) and convective boundary layer thickness (δ) at selected pressures (open triangles). Exponential fits to the calculated dissolution rates or distances are shown as dashed lines. The rate of quartz dissolution is dominated by the rate of diffusion of the slower eigencomponent (composition dominated by SiO_2) in the ternary system.

Overall, temperature and pressure have only a minor to moderate effect on the magnitude of coupled chemical diffusion for the melt compositions examined in this study.

4.2. Energetics of Chemical Diffusion

The diffusion matrix [**D**] is the product of a kinetic matrix [**L**] and a thermodynamic matrix [**G**] (e.g., Onsager, 1945; de Groot and Mazur, 1962; Haase, 1969):

$$\mathbf{[D] = [L] \cdot [G].} \tag{6}$$

With proper choice of a reference frame the elements of [**L**] satisfy Onsager's reciprocal relation $L_{ij} = L_{ji}$. The elements of [**G**] are functions of the derivatives of activity with respect to concentration. Both [**L**] and [**G**] matrices are positive definite for a single-phase liquid, which guarantees [**D**] to have positive eigenvalues (e.g., de Groot and Mazur, 1962; Haase, 1969). Unlike the elements of a diffusion matrix, the eigenvalues of [**D**] are independent of the choice of dependent variable. Hence it is convenient to study temperature and pressure dependence of the eigenvalues of [**D**]. For a ternary system, the major (λ_1) and minor (λ_2) eigenvalues of [**D**] are given by

$$\lambda_{1,2} = \frac{D_{11} + D_{22} \pm \sqrt{(D_{11} - D_{22})^2 + 4D_{12}D_{21}}}{2}, \tag{7}$$

where λ_2 takes the minus sign. Figures 5 and 6 display the calculated major (open circles) and minor (open squares) eigenvalues of the diffusion matrices as a function of pressure and reciprocal temperature for composition 7 and 12, respectively. The eigenvalues of [**D**] for the two melt compositions follow well-defined Arrhenius relationships with the reciprocal temperature (Figs. 5a and 6a). Table 3 lists the calculated activation energies for the two compositions at 1 GPa. These measured values are comparable to the activation energies for calcium and silicon self-diffusion at the same pressure and melt compositions (219 and 257 kJ mol^{-1} for self-diffusion of calcium and silicon in composition 7, and 211 and 197 kJ mol^{-1} for self-diffusion of calcium and silicon in composition 12 [Fig. 6a]; Liang et al., manuscript in preparation). This is very similar to previous studies of the energetics of self-diffusion and chemical diffusion in molten CAS at 1 bar and a melt composition of 40 wt.% CaO, 20% Al_2O_3, and 40% SiO_2 (composition 14 in Fig. 1; Towers and Chipman, 1957; Sugawara et al., 1977; Oishi et al., 1982). Variations in activation energies between compositions 7 and 12 are relatively small. The activation energies for composition 7 (60% SiO_2) are only 10% larger than the activation energies for composition 12, which has 45% SiO_2. At a given melt composition, the activation energy for λ_1 is ~12% smaller than the activation energy for λ_2. Consequently the ratios λ_1/λ_2 are not very sensitive to temperature variations (1440 to 1650°C), with an average of 5.5 ± 0.2 for composition 12 and an average of 3.7 ± 0.6 for composition 7.

The pressure dependence of [**D**] is quite different. At

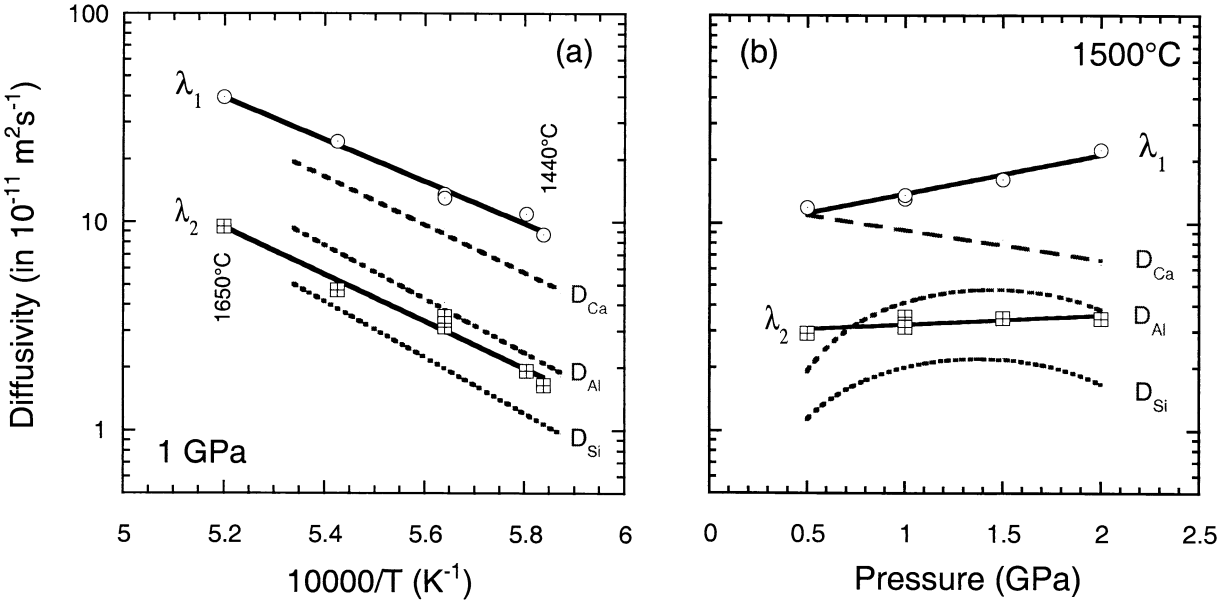

Fig. 6. Plots of major (λ_1, open circles) and minor (λ_2, squares) eigenvalues of diffusion matrices at composition 12 as a function of temperature (1 GPa, panel [a]) and pressure (1500°C, panel [b]). Exponential fits to the measured data are shown as solid lines. For comparison, best fit lines to measured calcium, aluminum, and silicon self-diffusion coefficients at the same melt composition, pressure (panel [a]) and temperature (panel [b]) are also shown (Liang et al., manuscript in preparation).

1500°C, the ratio λ_1/λ_2 increases with increasing pressure, with λ_1/λ_2 varying from 2.5 to 4.1 (0.5 to 1.3 GPa) for composition 7 and 4 to 6.5 (0.5 to 2.0 GPa) for composition 12. Figure 5b shows that λ_1 and λ_2 decrease with increasing pressure for composition 7, with activation volumes of 0.31×10^{-6} and 2.3×10^{-6} m^3 mol^{-1}, respectively (at 1500°C, Table 3). However, as shown in Figure 6b, λ_1 and λ_2 increase exponentially with increasing pressure for composition 12, with activation volumes of -1.48×10^{-6} and -0.42×10^{-6} m^3 mol^{-1}, respectively (at 1500°C). Despite the similarities in their dependence on temperature (Fig. 6a), the major and minor eigenvalues of [**D**] respond very differently to pressure changes than self-diffusivities of calcium and silicon for composition 12 (Fig. 6b). This is likely due to differences in structure and thermodynamic properties between the two melts.

To understand the energetics of multicomponent diffusion, we need to take a closer look at the relationship among [**D**], [**L**], and [**G**]. Differentiating Eqn. 6 with respect to temperature and pressure at a constant melt composition, we have

Table 3. List of activation energies and activation volumes.

Composition	E_1[a]	E_2	V_1[b]	V_2
7	215 ± 12	240 ± 21	0.31 ± 0.44	2.3 ± 0.8
12	192 ± 8	217 ± 14	–1.48 ± 0.18	–0.42 ± 0.24
Quartz dissolution	205		2.4	

[a] Activation energies, in kJ mol^{-1}, were calculated at 1 GPa.
[b] Activation volumes, in 10^{-6} m^3 mol^{-1}, were calculated at 1500°C. 1σ errors are also listed.

$$d[\boldsymbol{D}] = \left(\frac{\partial[\boldsymbol{D}]}{\partial T}\right)_{P,X} dT + \left(\frac{\partial[\boldsymbol{D}]}{\partial P}\right)_{T,X} dP = \left\{\left(\frac{\partial[\boldsymbol{L}]}{\partial T}\right)_{P,X} [\boldsymbol{G}] + [\boldsymbol{L}]\left(\frac{\partial[\boldsymbol{G}]}{\partial T}\right)_{P,X}\right\} dT + \left\{\left(\frac{\partial[\boldsymbol{L}]}{\partial P}\right)_{T,X} [\boldsymbol{G}] + [\boldsymbol{L}] \cdot \left(\frac{\partial[\boldsymbol{G}]}{\partial T}\right)_{T,X}\right\} dP. \quad (8)$$

To bare essential features of the energetics of chemical diffusion while keeping the analysis simple, we use a binary system below as an example. With component 2 as the dependent variable, Eqn. 6 can be written as (e.g., Darken, 1948; Cussler, 1984; Shewmon, 1989; Lasaga, 1998)

$$D_{11} = D_{11}^0\left(1 + \frac{\partial \ln \gamma_1}{\partial \ln X_1}\right) = D_{11}^0 I, \quad (9)$$

where D_{11} is the binary diffusion coefficient; X_1 and γ_1 are mole fraction and activity coefficient of component 1, respectively; and $I = 1 + \partial \ln \gamma_1 / \partial \ln X_1$ is the thermodynamic factor (e.g., Shewmon, 1989; Lasaga, 1998). $D_{11}^0 (= RTL_{11}/X_1)$ is the binary chemical diffusivity when the system is thermodynamically ideal ($I = 1$). Hence, at a constant melt composition, Eqn. 8 is reduced to

$$dD_{11} = \left(\frac{\partial D_{11}}{\partial T}\right)_P dT + \left(\frac{\partial D_{11}}{\partial P}\right)_T dP, \quad (10a)$$

where the temperature and pressure derivatives are

$$\left(\frac{\partial D_{11}}{\partial T}\right)_P = I\left(\frac{\partial D_{11}^0}{\partial T}\right)_P - \frac{D_{11}^0}{RT^2}\left(\frac{\partial H_1}{\partial \ln X_1}\right)_T, \quad (10b)$$

$$\left(\frac{\partial D_{11}}{\partial P}\right)_T = I\left(\frac{\partial D_{11}^0}{\partial P}\right)_T - \frac{D_{11}^0}{RT}\left(\frac{\partial V_1}{\partial \ln X_1}\right)_P. \quad (10c)$$

H_1 and V_1 are partial molar enthalpy and partial molar volume of component 1, respectively. The second terms on the right-hand side of Eqn. 10b and 10c were obtained using the standard thermodynamic relationships (e.g., Denbigh, 1981)

$$\left(\frac{\partial \ln \gamma_1}{\partial P}\right)_{T,C_1} = \frac{V_1 - V_1^0}{RT}$$

and

$$\left(\frac{\partial \ln \gamma_1}{\partial T}\right)_{P,C_1} = -\frac{H_1 - H_1^0}{RT^2},$$

where V_1^0 and H_1^0 are partial molar enthalpy and partial molar volume of component 1 at its standard state, respectively.

According to empirical models for multicomponent diffusion, D_{11}^0 is a function of self-diffusion coefficients, melt composition, cation and anion charge numbers, and, to a lesser extent, partial molar volumes of the components in the system (e.g., Darken, 1948; Cooper, 1965; Oishi, 1965; Lasaga, 1979; Richter, 1993; Zhang, 1993; Liang et al., 1997). In the simplest form it can be written as

$$D_{11}^0 = (1 - X_1) D_1 + X_1 D_2, \quad (11)$$

where D_1 and D_2 are self-diffusion coefficients of components 1 and 2, respectively (e.g., Darken, 1948; similar but more complete expressions for ionic melts can be found in Liang et al., 1997). It is well known that self-diffusion coefficient depends exponentially on temperature and pressure. Hence, it is reasonable to assume that D_{11}^0 follows a similar exponential relationship, namely,

$$D_{11}^0 = D_0 \exp\left(-\frac{E_a + PV_a}{RT}\right), \quad (12)$$

where D_0 is the preexponential factor and E_a and V_a are activation energy and activation volume for chemical diffusion when the liquid is thermodynamically ideal. To a good approximation, we expect that the magnitudes of E_a and V_a are bounded by the activation energies and activation volumes for self-diffusion of the components in the system (e.g., Sugawara et al., 1977; also see Fig. 6). Substituting Eqn. 12 into Eqn. 10b and 10c, after rearranging, we have

$$\left(\frac{\partial \ln D_{11}}{\partial T}\right)_P = \frac{1}{RT^2}\left[E_a + PV_a - \frac{1}{I}\left(\frac{\partial H_1}{\partial \ln X_1}\right)_T\right], \quad (13a)$$

$$\left(\frac{\partial \ln D_{11}}{\partial P}\right)_T = \frac{1}{RT}\left[V_a - \frac{1}{I}\left(\frac{\partial V_1}{\partial \ln X_1}\right)_P\right]. \quad (13b)$$

The terms in the square brackets in Eqn. 13a and 13b are equal to the activation energy (at a constant pressure) and activation volume (at a constant temperature), respectively, for chemical diffusion in the binary liquid. The denominators in the last terms in the square brackets in Eqn. 13a and 13b account for thermodynamic nonideality of the melt. Hence, similarities in activation energies between chemical diffusion and self-diffusion imply that the enthalpy of melt is not a strong function of composition in molten CAS. The contrasting behavior in pressure dependence between chemical diffusion and self-diffusion suggests that the partial molar volume of melt in CAS may be a strong function of melt composition. A detailed analysis of the relationships among the energetics of self-diffusion, chemical diffusion, and thermodynamic properties of the melt in CAS will be presented in a companion paper in which the energetics of self-diffusion will be discussed.

4.3. Comparison with Prevision Studies

A comparison of the major and minor eigenvectors of [**D**] for the two melt compositions revealed that they are not very sensitive to temperature and pressure variations. For the temperature and pressure ranges examined in this study (1440 to 1650°C at 1 GPa and 0.5 to 2.0 GPa at 1500°C), average values of the major and minor eigendirections are -0.67 ± 0.09 and -0.62 ± 0.9, respectively, for composition 7 and -0.55 ± 0.11 and 2.4 ± 0.2 for composition 12. Major eigendirection is defined as $(D_{11} - \lambda_1)/D_{12}$, and minor eigendirection is given by $(D_{11} - \lambda_2)/D_{12}$. This is consistent with observations of weak temperature dependence of the eigenvectors of [**D**] in simple molten systems such as K_2O-CaO-SiO_2 (Engelke, 1972), K_2O-SrO-SiO_2 (Varshneya and Cooper, 1972), K_2O-Al_2O_3-SiO_2 (Chakraborty et al., 1995), CAS (Sugawara et al., 1977; Oishi et al., 1982), CMAS (Liang and Richter, unpublished data), and K_2O-NaO-Al_2O_3-SiO_2-H_2O (Mungall et al., 1998).

Figure 7 compares our measured eigenvalues of [**D**] in molten CAS at 1 GPa with eigenvalues of [**D**] in molten CAS (Sugawara et al., 1977; composition 14 in Fig. 1) for two compositions in molten K_2O-Al_2O_3-SiO_2 (Chakraborty et al., 1995) and one composition in molten CMAS (Liang and Richter, unpublished data), all at 1 bar. At a given temperature (say 1500°C), diffusivities span over 5 orders of magnitude. Eigenvalues of [**D**] in molten CAS, CMAS, and MgO-Al_2O_3-SiO_2 (Richter et al., 1998), are 1 to 4 orders of magnitude higher than those in molten K_2O-Al_2O_3-SiO_2. Clearly, melt composition and structure are the dominant factors in determining the activation energies and magnitudes of the eigenvalues of diffusion matrices in these simple systems.

5. GEOLOGICAL APPLICATIONS

The diffusion matrices obtained from this study can be used to model various mass transfer processes in molten or partially molten CAS, which is one of the simplest multicomponent systems that has some of the key components of natural magmas. As an example, we show below how the experimentally determined chemical diffusion coefficients can be used to calculate the activation energy and activation volume of crystal dissolution in this analog system. For simplicity, we consider the rate of diffusive dissolution of a quartz crystal or a pure quartzite in a CAS melt as a function a temperature and pressure. The dissolving melt is a haplobasaltic-andesitic liquid with 30 wt.% CaO, 20% Al_2O_3, and 50% SiO_2 (composition 16

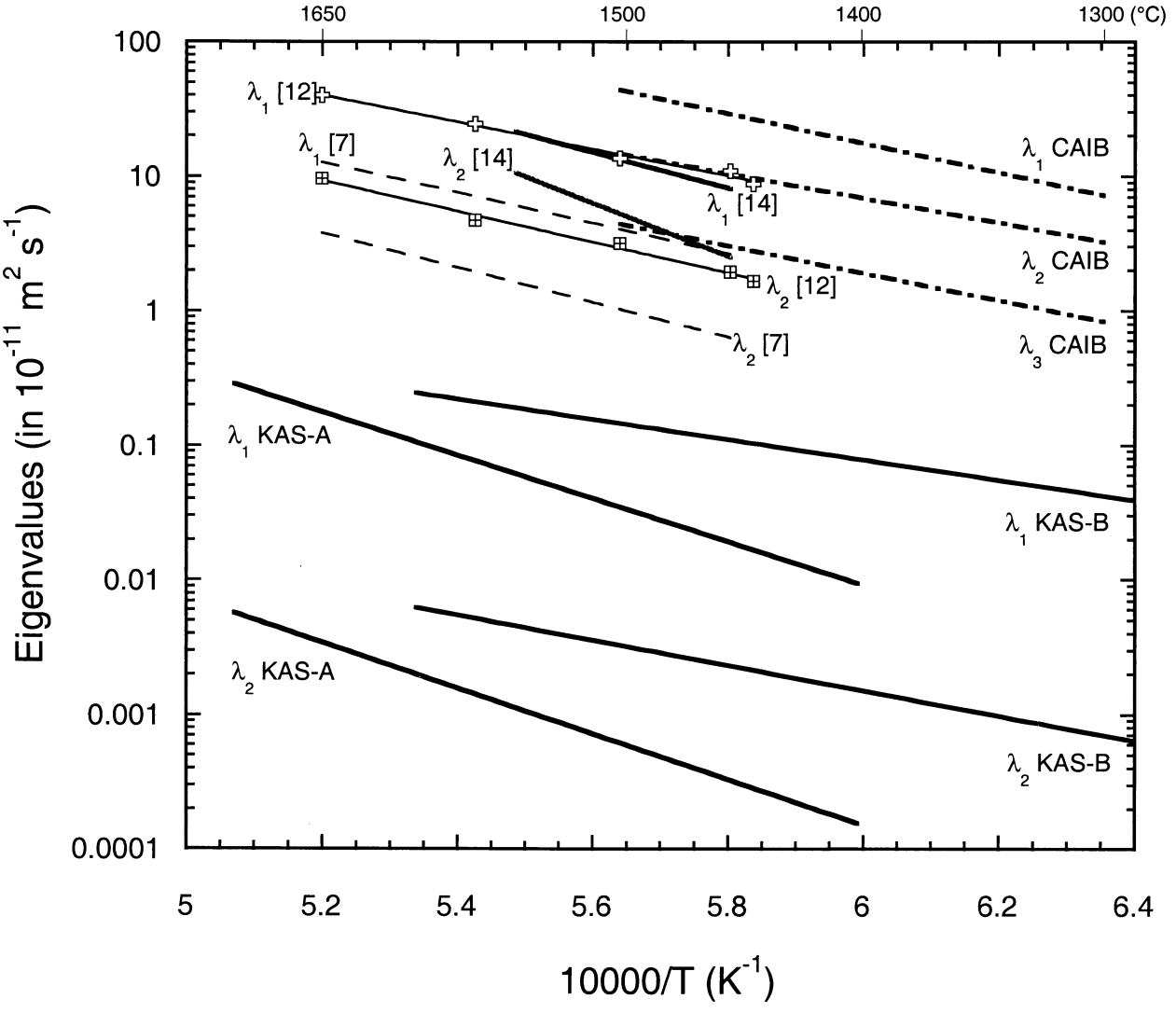

Fig. 7. Plots of eigenvalues of diffusion matrices in selected ternary and quaternary systems as a function of the reciprocal temperature. Three compositions in CaO-Al_2O_3-SiO_2: compositions 7, 12 (this study, at 1 GPa), and 14 (40 wt.% CaO, 20% Al_2O_3, 40% SiO_2, 1 bar, Sugawara et al., 1977). Two compositions in K_2O-Al_2O_3-SiO_2 (KAS) (Chakraborty et al., 1995, at 1 bar): KAS-A (9% K_2O, 16% Al_2O_3, 75% SiO_2) and KAS-B (16% K_2O, 9% Al_2O_3, 75% SiO_2). One composition in CaO-MgO-Al_2O_3-SiO_2 (labeled CAIB): 33% CaO, 8% MgO, 25% Al_2O_3, 34% SiO_2. Diffusion matrices in the CAIB melts were calculated at 1 bar using the ionic common-force model of Liang et al. (1997), the activity model of Berman (1983), and self diffusivities from the literature.

in Fig. 1). The SiO_2 content at the crystal-melt interface, calculated from experimentally measured quartz liquidus (see below), varies between 65 and 75% at the temperature and pressure ranges considered (1375 to 1500°C at 1 GPa and 0.5 to 1.6 GPa at 1500°C). Hence, diffusion matrices at composition 7 can be used as an approximation in our dissolution calculations. Also, for simplicity, we choose a one-dimensional, effectively semi-infinite dissolution couple at a constant temperature and pressure. For such a setup, we have shown previously that dissolution distance and melt compositions at the crystal-melt interface at a given time can be calculated given the liquidus surface of the dissolving crystal, composition of the starting melt, and elements of the diffusion matrix (Liang, 1999). The dissolution distance, X_b, is given by the usual expression

$$X_b = 2\alpha\sqrt{\lambda_1 t}, \tag{14}$$

where α is a dimensionless dissolution parameter and can be calculated exactly using Eqn. 1h and 3a to 3c in Liang (1999). In the case of slow dissolution, the dissolution parameter can be calculated using the approximate expression

$$\alpha \approx -0.7763\Phi\left(1 - \sqrt{1 + 1.4535\frac{\Theta}{\Phi}}\right)\varepsilon, \tag{15a}$$

where the three dimensionless parameters Φ, Θ, and ε are

Table 4. List of quartz liquidus compositions.

Run	T (°C)	P (GPa)	CaO (wt.%)	Al_2O_3 (wt.%)	SiO_2 (wt.%)	Duration (h)
QZLIQ5	1500	0.5	12.97 ± 0.12	10.42 ± 0.11	76.61 ± 0.18	25.3
QZLIQ5	1500	0.5	17.63 ± 0.18	8.78 ± 0.10	73.59 ± 0.24	25.3
QZLIQ6	1500	1.6	24.61 ± 0.22	12.37 ± 0.11	63.02 ± 0.29	48.9
QZLIQ6	1500	1.6	20.30 ± 0.22	16.44 ± 0.15	63.26 ± 0.26	48.9
QZLIQ6	1500	1.6	24.81 ± 0.32	12.41 ± 0.19	62.78 ± 0.47	48.9
QZLIQ6	1500	1.6	20.29 ± 0.14	16.46 ± 0.08	63.25 ± 0.14	48.9
QZLIQ7	1500	1.6	20.03 ± 0.28	16.16 ± 0.24	63.81 ± 0.49	50.1
QZLIQ7	1500	1.6	24.25 ± 0.38	12.29 ± 0.30	63.46 ± 0.66	50.1
QZLIQ3	1375	1.0	20.04 ± 0.19	16.19 ± 0.12	63.76 ± 0.24	70.3
QZLIQ3	1375	1.0	24.48 ± 0.19	12.29 ± 0.09	63.23 ± 0.20	70.3
Q4B-4Q2	1375	1.0	20.67 ± 0.27	16.09 ± 0.20	63.24 ± 0.42	51.3

Liquidus[a]	*T*	*P*	p_1	p_2	*s*
	1500	0.5	0.64856	1.0	0.85020
	1500	1.0[b]	0.21040	1.0	0.71375
	1500	1.6	0.090731	1.0	0.65294
	1375	1.0	0.079344	1.0	0.65136

Concentrations from an average of 5 to 20 analyses of glasses coexisting with quartz.

[a] Coefficients for the liquidus Eqn. 15e were calculated from least squares fits to the measured liquidus data.

[b] From Liang (1999). The bulk compositions of the starting mixtures are well within the expected quartz primary fields. Each run was first held at 1600°C and a desired pressure for 0.5 h. The temperature was then decreased to a desired run temperature (second column) at 1°C min^{-1} and held at the run there for the duration indicated (last column).

$$\Phi = \frac{1 + k\varepsilon}{1 + k\varepsilon^2},\ \Theta = \frac{s - C_{11}p_1 - C_{21}p_2}{A_1\varepsilon + A_2},\ \varepsilon = \sqrt{\frac{\lambda_2}{\lambda_1}},\ k = \frac{A_1}{A_2}, \tag{15b}$$

$$A_1 = \frac{1}{\lambda_1 - \lambda_2}\{[p_1(D_{11} - \lambda_2) + p_2D_{21}](C_{11} - C_{s1}) + [p_1D_{12} + p_2(D_{22} - \lambda_2)](C_{21} - C_{s2})\}, \tag{15c}$$

$$A_2 = \frac{1}{\lambda_1 - \lambda_2}\{[p_1(D_{11} - \lambda_1) + p_2D_{21}](C_{11} - C_{s1}) + [p_1D_{12} + p_2(D_{22} - \lambda_1)](C_{21} - C_{s2})\}, \tag{15d}$$

p_1, p_2, and s are coefficients of the linearized quartz liquidus given by

$$p_1C_{10} + p_2C_{20} = s, \tag{15e}$$

and C_{10} and C_{20} are melt composition at the crystal-melt interface and can be calculated from Eqn. 3a to 3c in Liang (1999) once α is known. Eqn. 15a provides a good approximation to the dissolution parameter α when $|\Theta/\Phi|<0.6$. Φ is of order 1 and Θ is a measure of the degree of undersaturation in the liquid. An important assumption used in the derivation of Eqn. 14 is that crystal and melt are in thermodynamic equilibrium at their interface during the course of dissolution. We have shown experimentally that this is a valid assumption for quartz dissolution in molten CAS at 1500°C and 1 GPa (Liang, 1999).

To calculate dissolution distances, the quartz liquidus was experimentally determined at 1500°C and 0.5, 1.0, and 1.6 GPa and at 1375°C and 1 GPa by equilibrating mixtures of fine-grained quartz and glass powders of selected compositions in the ternary system CAS following previously described procedures (Liang, 1999; also briefly summarized in the footnote to Table 4). Table 4 summarizes results of electron microprobe analysis of melts coexisting with quartz at the temperatures and pressures examined. Coefficients for the linearized quartz liquidus are listed in Table 4. Figures 5a and 5b display the normalized dissolution distances, $X_b/\sqrt{t}$, calculated using Eqn. 15a to 15d with experimentally determined liquidus and diffusion matrices at composition 7, as a function of pressure and reciprocal temperature (dashed lines through filled circles). The calculated activation energy and activation volume for quartz dissolution at this melt composition are slightly different from the measured activation energy and activation volume for chemical diffusion of the minor or slow eigencomponent of the system (Table 3). This is because quartz liquidus is also a function of temperature and pressure (see Table 4). However, such small differences, though real, are within the uncertainties of the measured activation energy and activation volume for chemical diffusion and crystal dissolution and hence are unlikely to be detected from experimental measurements. Nevertheless, Figures 5a and especially 5b show quite convincingly that the crystal dissolution rate is dominated by the diffusion rate of the slow eigencomponent in the system, a conclusion consistent with many previous crystal dissolution studies (e.g., Watson, 1982; Harrison and Watson, 1983; Zhang et al., 1989; Woods, 1992; Liang, 1999). As will be shown elsewhere, this conclusion is also true for convective crystal dissolution when hydrodynamic factors are held constant. An example of the calculated products of quartz convective dissolution rate (V) and convective boundary layer thickness (δ) at selected pressures is given in Figure 5b (open triangles joined by dashed line). The convective boundary layer thickness depends weakly on diffusivity and melt viscosity when the convective flow is laminar (e.g., Kerr, 1995).

6. CONCLUSIONS

The temperature and pressure dependence of the elements of diffusion matrices for two melts in the ternary system CAS

were examined at pressures of 0.5 to 2 GPa and temperatures of 1440 to 1650°C. Diffusion matrices were measured in a mass-fixed frame of reference with simple oxides CaO, Al_2O_3, and SiO_2 as end-member components and Al_2O_3 as the dependent variable. To a good approximation, temperature and pressure dependence of the measured diffusion matrices can be parameterized by simple exponential relationships. In general, a change in temperature of 100°C results in a relative change in elements of diffusion matrix of 50 to 100%, whereas a change in pressure of 1 GPa introduces a relative change in elements of diffusion matrix of less than 12%. Major and minor eigenvalues of the diffusion matrices follow well-defined Arrhenius relationships with the pressure and reciprocal temperature. At 1 GPa, activation energies for the eigenvalues of the diffusion matrices are comparable to the activation energies for self-diffusion of Ca and Si at the same melt compositions. At 1500°C, activation volumes for the eigenvalues of the diffusion matrices, though small, are quite different between the two melts. This difference is likely a result of a difference in the thermodynamic properties of the melt (e.g., partial molar volume).

Chemical diffusion in molten CAS shows clear evidence of strong diffusive coupling among the components. Results from this study further support our earlier conclusions that the flux of SiO_2 is strongly coupled to the concentration gradients of CaO (and perhaps MgO, FeO, Na_2O, and K_2O as well) in melts of more siliceous compositions in natural magmas (rhyolitic-andesitic compositions). For a given melt composition, coupled chemical diffusion, hence directions of eigenvectors of [**D**], are not very sensitive to temperature and pressure variations.

Applications of our measured diffusion matrices to quartz crystal dissolution in molten CAS reveal that the activation energy and activation volume for quartz dissolution are almost identical to the activation energy and activation volume for diffusion of the minor or slower eigencomponent of the diffusion matrix. This conclusion is likely to be valid for crystal growth and dissolution in natural magmas when diffusion in liquid is the rate-limiting factor.

Acknowledgments—We wish to thank Frank M. Richter and E. Bruce Watson for their advice and many suggestions throughout the course of this study. This paper benefited from the constructive reviews of Bruno Giletti and official reviews of Don Baker and Jim Mungall. This work was supported by Department of Energy grant DE-FG02-94ER14478 to F. M. Richter, NASA grant NAG5-9510 to A. M. Davis, and National Science Foundation grants EAR-940691 to E. B. Watson and EAR-9903020 to Y. Liang.

Associate editor: F. J. Ryerson

REFERENCES

Ayers J. C., Brenan J. B., Watson E. B., Wark D. A., and Minarik W. G. (1992) A new capsule technique for hydrothermal experiments using the piston-cylinder apparatus. *Am. Mineral.* **77,** 1080–1086.

Berman R. G. (1983) *A thermodynamic model for multicomponent melts, with application to the system CaO-MgO-Al_2O_3-SiO_2.* Ph.D. thesis, University of British Columbia.

Chakraborty S., Dingwell D. B., and Rubie D. C. (1995) Multicomponent diffusion in ternary silicate melts in the system K_2O-Al_2O_3-SiO_2: I. Experimental measurements. *Geochim. Cosmochim. Acta* **59,** 255–264.

Cooper A. R. (1965) Model for multi-component diffusion. *Phys. Chem. Glasses* **6,** 55–61.

Cooper A. R., Jr., and Kingery W. D. (1964) Dissolution in ceramic systems: I. Molecular diffusion, natural convection, and forced convection studies of sapphire dissolution in calcium aluminum silicate. *J. Am. Ceram. Soc.* **47,** 37–43.

Cussler E. L. (1984) *Diffusion Mass Transfer in Fluid Systems*. Cambridge University Press, New York.

Darken L. S. (1948) Diffusion, mobility and their interrelation through free energy in binary metallic systems. *Trans. Metall. Soc. AIME* **175,** 184–201.

de Groot S. R. and Mazur P. (1962) *Non-Equilibrium Thermodynamics*. Dover, New York.

Denbigh K. (1981) *The Principles of Chemical Equilibrium*. Cambridge University Press, Cambridge, UK.

Engelke H. (1972) *Chemische diffusion und brechungsindexverlauf in zuasmmengeschmolzenen gläsern*. Thesis, Universität Erlangen-Nürnberg.

Fujita H. and Gosting L. J. (1956) An exact solution of the equations for free diffusion in three-component systems with interacting flows, and its use in evaluation of the diffusion coefficients. *J. Am. Chem. Soc.* **78,** 1099–1106.

Harrison T. M. and Watson E. B. (1983) Kinetics of zircon dissolution and zirconium diffusion in granitic melts of variable water content. *Contrib. Mineral. Petrol.* **84,** 66–72.

Haase R. (1969) *Thermodynamics of Irreversible Processes*. Dover, New York.

Kerr R. C. (1995) Convective crystal dissolution. *Contrib. Mineral. Petrol.* **121,** 237–246.

Kirkaldy J. S. (1958) Diffusion in multicomponent metallic systems: I. Phenomenological theory for substitutional solid solution alloys. *Can. J. Phys.* **36,** 899–906.

Kress V. C. and Ghiorso M. S. (1993) Multicomponent diffusion in MgO-Al_2O_3-SiO_2 and CaO-MgO-Al_2O_3-SiO_2 melts. *Geochim. Cosmochim. Acta* **57,** 4453–4466.

Lasaga A. C. (1979) Multicomponent exchange and diffusion in silicates. *Geochim. Cosmochim. Acta* **43,** 455–469.

Lasaga A. C. (1998) *Kinetic Theory in the Earth Sciences*. Princeton University Press, Princeton, NJ.

Liang Y. (1994) *Models and experiments for multicomponent chemical diffusion in molten silicates*. Ph.D. thesis, University of Chicago.

Liang Y. (1999) Diffusive dissolution in ternary systems: Analysis with applications to quartz and quartzite dissolution in molten silicates. *Geochim. Cosmochim. Acta* **63,** 3983–3995.

Liang Y. (2000). Dissolution in molten silicates: Effects of solid solution. *Geochim. Cosmochim. Acta* **64,** 1617–1627.

Liang Y., Richter F. M., Davis A. M., and Watson E. B. (1996a) Diffusion in silicate melts: I. Self diffusion in CaO-SiO_2-Al_2O_3 at 1500°C and 1 GPa. *Geochim. Cosmochim. Acta* **60,** 4353–4367.

Liang Y., Richter F. M., and Watson E. B. (1996b) Diffusion in silicate melts: II. Multicomponent diffusion in CaO-SiO_2-Al_2O_3 at 1500°C and 1 GPa. *Geochim. Cosmochim. Acta* **60,** 5021–5035.

Liang Y., Richter F. M., and Chamberlin L. (1997) Diffusion in silicate melts: III. Empirical models for multicomponent diffusion. *Geochim. Cosmochim. Acta* **61,** 5295–5312.

Mungall J. E., Romano C., and Dingwell D. B. (1998) Multicomponent diffusion in molten system K_2O-Na_2O-Al_2O_3-H_2O. *Am. Mineral.* **83,** 685–699.

Oishi Y. (1965) Analysis of ternary diffusion: Solutions of diffusion equations and calculated concentration distribution. *J. Chem. Phys.* **43,** 1611–1620.

Oishi Y., Nanba M., and Pask J. A. (1982) Analysis of liquid-state interdiffusion in the system CaO-Al_2O_3-SiO_2 using multiatomic ion models. *J. Am. Ceram. Soc.* **65,** 247–253.

Onsager L. (1945) Theories and problems of liquid diffusion. *Ann. New York Acad. Sci.* **46,** 241–265.

Richter F. M. (1993) A method for determining activity-composition relations using chemical diffusion in silicate melts. *Geochim. Cosmochim. Acta* **57,** 2019–2032.

Richter F. M., Liang Y., and Minarik W. G. (1998) Multicomponent diffusion and convection in molten MgO-Al_2O_3-SiO_2. *Geochim. Cosmochim. Acta* **62,** 1985–1991.

Shewmon P. (1989) *Diffusion in Solids*. The Minerals, Metals & Materials Society, Warrendale, PA.

Sugawara H., Nagata K., and Goto K. S. (1977) Interdiffusivities matrix of CaO-Al_2O_3-SiO_2 melt at 1723 K to 1823 K. *Metall. Trans.* **8B,** 605–612.

Towers H. and Chipman J. (1957) Diffusion of calcium and silicon in a lime-alumina-silica slag. Trans. Metall. Soc. AIME. 209, 769–773.

Trial A. F. and Spera F. J. (1994) Measuring the multicomponent diffusion matrix: Experimental design and data analysis for silicate melts. *Geochim. Cosmochim. Acta* **58,** 3769–3783.

Varshneya A. K. and Cooper A. R. (1972) Diffusion in the system K_2O-SrO-SiO_2: III. Interdiffusion coefficients. *J. Am. Ceram. Soc.* **55,** 312–317.

Wakabayashi H. and Oishi Y. (1978) Liquid-state diffusion of Na_2O-CaO-SiO_2. *J. Chem. Phys.* **68,** 2046–2052.

Watson E. B. (1982) Basalt contamination by continental crust: Some experiments and models. *Contrib. Mineral. Petrol.* **80,** 73–87.

Watson E. B. and Baker D. R. (1991) Chemical diffusion in magmas: An overview of experimental results and geochemical applications. In *Physical Chemistry of Magmas* (eds. L. L. Perchuk and I. Kushiro), pp. 120–151. Springer-Verlag, New York.

Woods A. W. (1992) Melting and dissolving. *J. Fluid Mech.* **239,** 429–448.

Zhang Y. (1993) A modified effective binary diffusion model. *J. Geophys. Res.* **98,** 11901–11920.

Zhang Y., Walker D., and Lesher C. E. (1989) Diffusive crystal dissolution. *Contrib. Mineral. Petrol.* **102,** 492–513.